RSC Advances

PAPER

View Article Online
View Journal | View Issue

Cite this: *RSC Adv.*, 2025, **15**, 27723

Phytofabrication of Ag/AgCl silver nanoparticles from the extract of *Phoenix dactylifera* L. Medjool date seeds: synthesis, characterization and antimicrobial properties†

Pushpa Thirubuvanesvari-Duraivelu, [a] Siti Salwa Abd Gani, *[ab] Masriana Hassan,[c] Mohd Izuan Effendi Halmi,[d] Reem Fawaz Abutayeh, [e] Mohammad A. A. Al-Najjar [e] and Ala' Abu-Odeh[e]

The persistence of biofilm-associated infections in skin and soft tissues poses a significant challenge in clinical settings, necessitating the development of sustainable alternatives to conventional antimicrobial agents, paired with development of eco-friendly and non-toxic nanomaterials. This study reports phytofabrication of Ag/AgCl nanoparticles (Ag/AgCl-NPs) using ultrasonicated 80% ethanolic extract of *Phoenix dactylifera* L. Medjool date seeds (MdSE) without using any external reagents, leveraging their rich phytochemical content as natural reducing and stabilizing agents. The synthesized nanoparticles were characterized using UV-visible spectroscopy (UV-vis), field emission scanning electron microscopy (FESEM), high-resolution field emission transmission electron microscopy (HR-FETEM), selected area electron diffraction (SAED), X-ray diffraction (XRD), and energy-dispersive X-ray (EDX) confirming their average size of 16.75 ± 7.25 nm, spherical morphology, crystalline structure, face-centered cubic (fcc) phase, silver and chlorine entities, and high colloidal stability. Phytochemical screening *via* Fourier transform infrared spectroscopy (FTIR) analysis identified polyphenols, flavonoid, and protein as the key contributors to the reduction of Ag^{+} ions to Ag^{0} species, leading to the successful formation of MdSE-Ag/AgCl-NPs. The antimicrobial efficacy of the nanoparticles was evaluated against two pathogenic Gram-negative bacteria (*Escherichia coli* and *Pseudomonas aeruginosa*) and one Gram-positive bacteria (*Staphylococcus aureus*). The synthesized nanoparticles exhibited significant antibacterial activity, with substantial inhibition of bacterial biofilm formation, especially in reducing biofilm development by 73.57% for *P. aeruginosa* and 88.66% for *S. aureus* at 1*MIC, respectively. The synthesized MdSE-Ag/AgCl-NPs exhibit promising characteristics, supporting the effectiveness of Medjool seeds as a bioreductant in nanoparticle synthesis. Their notable properties suggest potential applications in modern medicine and clinical applications, particularly for biofilm prevention and management.

Received 29th April 2025
Accepted 31st May 2025

DOI: 10.1039/d5ra03020j

rsc.li/rsc-advances

Introduction

Skin and soft tissue infections are among the most common clinical challenges, often caused by bacterial pathogens such as *Escherichia coli*, *Pseudomonas aeruginosa*, and *Staphylococcus aureus*. These infections range in severity from superficial wounds to deep abscesses and life-threatening necrotizing fasciitis. The onset of the infection typically involves microbial invasion into skin and underlying tissue layers, triggering a cascade of host immune responses. The progression of these infections is driven by an intricate interplay between microbial virulence and host immune mechanisms, further intensified by oxidative damage, inflammation, and delayed tissue regeneration. The key obstacle in their management is the emergence of antibiotic resistance, coupled with the ability of these bacteria to form biofilms layers, which is a dense matrix of extracellular polymeric substances that protect microbial cells from both immune responses and antimicrobial agents. Biofilm-associated infections are notoriously persistent and contribute significantly to chronic wound complications, delayed healing,

[a]*Natural Medicine and Product Research Laboratories (NaturMeds), Institute of Bioscience (IBS), Universiti Putra Malaysia, 43400 Serdang, Selangor, Malaysia. E-mail: ssalwaag@upm.edu.my*

[b]*Department of Agriculture Technology, Faculty of Agriculture, Universiti Putra Malaysia (UPM), 43400 Serdang, Selangor, Malaysia*

[c]*Department of Pathology, Faculty of Medicine and Health Sciences, Universiti Putra Malaysia (UPM), 43400 Serdang, Selangor, Malaysia*

[d]*Department of Land Management, Faculty of Agriculture, Universiti Putra Malaysia (UPM), 43400 Serdang, Selangor, Malaysia*

[e]*Department of Pharmaceutical Chemistry and Pharmacognosy, Faculty of Pharmacy, Applied Science Private University (ASU), 11937 Amman, Jordan*

† Electronic supplementary information (ESI) available. See DOI: https://doi.org/10.1039/d5ra03020j

treatment failure, and increased mortality, eventually leading to increased healthcare burdens and higher treatment costs.[1]

This growing resistance crisis has spurred global interest in alternative therapeutic strategies that are both sustainable and cost-effective. Nanotechnology, particularly the application of metal-based nanoparticles, has emerged as a powerful tool, offering unique advantages over their macroscopic counterparts. Historically, silver has earned a significant role as a "dynamic" and "biocidal therapeutic agent" in medicine, celebrated for its broad-spectrum biological capabilities.[2] Clinically, it has been widely used in formulations like silver sulfadiazine for managing skin infections and traditional healing systems such as Ayurveda have long employed silver-based remedies to manage infectious conditions.[3,4] Notably, silver has been reported to combat over 650 disease-causing microorganisms, further underscoring its therapeutic versatility.[5,6] The convergence of this traditional wisdom with modern nanotechnology offers new avenues for treating skin and soft tissue infections, especially in an era of rising antibiotic resistance.

At nanoscale, silver nanoparticles (AgNPs) are widely recognized for their broad-spectrum antimicrobial efficacy, including action against multi-drug-resistant strains. They are particularly favoured for minimizing the risk of resistance development due to their ability to target multiple bacterial pathways simultaneously. Owing to their nanoscale dimensions, silver nanoparticles can directly interact with microbial membranes and biofilms, compromising cellular integrity and disrupting their metabolic processes. A reduction in particle size leads to a higher surface-to-volume ratio, which enhances their dispersion and significantly amplifies their antimicrobial potency.[7] In addition to their bactericidal potential, these nanomaterials possess anti-inflammatory, antioxidant, and anticancer properties, which are the traits that have expanded their application across various domains of nanomedicine.[8,9]

Beyond AgNPs, recent studies have documented the successful biosynthesis of hybrid silver/silver chloride nanoparticles (Ag/AgCl-NPs) relying solely on silver nitrate ($AgNO_3$) and phytochemicals from plant extracts to drive both reduction and stabilization.[10–12] These studies demonstrated the phytofabrication of Ag/AgCl-NPs without the addition of external chloride sources. The plasmonic nanohybrids exhibited enhanced antibacterial activity *via* its ability to generate reactive oxygen species (ROS) under light exposure[13,14] and anticancer performance[15] with comparatively low cytotoxicity such as in HeLa cells,[16] a feature likely attributed to the controlled solubility equilibrium of Ag^+ ions regulated by the presence of AgCl. This ensures a sustained but minimal release of silver ions into the environment.[17] Current study aims to contribute to this growing body of research by demonstrating Ag/AgCl nanohybrids synthesized *via* a green route not only retain a strong antibacterial and antibiofilm performances, but are also suitable for therapeutic potential combating bacterial infections, such as in antibacterial coatings and wound dressings.

Among various botanicals explored for green nanomaterial synthesis, the date palm (*Phoenix dactylifera* L.), particularly its Medjool variety, has emerged as a promising yet underexploited resource. With global production exceeding 9.82 million metric tons in 2023 alone[18] and being an important player in the market, an estimated 900 000 tons of date seeds are generated annually, yet most are discarded or used as animal feed due to limited awareness of their potential value. The Medjool variety experimented in this study known as the "King of Dates" is one of the finest cultivars and are prized for their large, soft texture, and exceptional quality.[19] They are widely cultivated in arid regions such as the Middle East and North Africa. This agricultural by-product is rich in bioactive compounds, including polyphenols, flavonoids, phenolic acids, and dietary fibres making it a compelling candidate for sustainable applications.[20,21] Impressively, their antioxidant capacity exceeds that of the fruit pulp by containing up to 18 times more gallic acid equivalents and 4–7 times more Trolox equivalents per 100 g.[22] Recent studies have proposed the use of date seeds, including Ajwa and Rothan varieties, as green reducing agents in the synthesis of silver nanoparticles (AgNPs), with promising outcomes in antibacterial, antifungal, reducing cancer proliferation, and anti-inflammatory activity.[23–25] However, Medjool variant remains underexplored. Harnessing the phytochemical richness of Medjool date seeds for phytofabrication presents a sustainable strategy that repurposes agricultural wastes into high-value biomedical materials.

In this study, we report the phytofabrication of Ag/AgCl-NPs using ultrasonicated ethanolic extract of Medjool date seeds (MdSE). The synthesized nanomaterials were characterized using multiple analytical techniques to confirm their structural, morphological, and elemental properties. The antibacterial potential of the biosynthesized silver/silver chloride nanoparticle from MdSE (MdSE-Ag/AgCl-NPs) was evaluated against three clinically relevant bacterial strains, namely *E. coli*, *P. aeruginosa*, and *S. aureus*. These pathogens are commonly implicated in skin and soft tissue infections, and known for their biofilm-forming capabilities. Additionally, the antibiofilm activity of these nanoparticles was assessed to determine their potential in disrupting bacterial biofilms, providing insights into their prospect as alternative therapeutics for biofilm-associated infections.

Experimental

Retrieval and preparation of *P. dactylifera* L. Medjool seeds extract

A modified extraction protocol was utilized to prepare Medjool date seeds (MdS) powder following Thirubuvanesvari-Duraivelu *et al.* (2024).[26] The seeds were separated from the fruit, thoroughly washed to remove residual pulp, and subjected to oven drying at 45 °C for 24 hours. Once dried, the seeds were finely ground using a high-powered grinder, and the resulting powder was sieved through a 1–2 mm mesh to achieve uniform particle size.

For extraction, 2 g of MdS powder was mixed with 100 mL of 80% ethanol and processed *via* ultrasound-assisted extraction (UAE) using a sonication water bath (Elmasonic S60 H, Elma Hans Schmidbauer GmbH, Singen, Germany) at 70 °C for 40 minutes, facilitating the release of bioactive compounds. The

extract was then subjected to centrifugation at 3000 rpm for 5 minutes to remove insoluble residues, followed by vacuum filtration with Whatman No. 1 filter paper to eliminate particulates.

To ensure the preservation of phytochemical constituents, solvent removal was performed using a rotary evaporator at 45 °C, preventing thermal degradation. The resulting Medjool date seeds extract (MdSE) was stored in glass vials at −20 °C until further application in the phytofabrication of silver/silver chloride nanoparticles.

Phytofabrication of Ag/AgCl-NPs using MdSE

The phytofabrication of Ag/AgCl-NPs was achieved using Medjool date seeds extract, which served as a natural reducing and stabilizing agent. An aqueous solution of 1 mM silver nitrate ($AgNO_3$) was prepared in deionized water and combined with the MdSE at 1 mg mL^{-1} in an equal 1 : 1 volume ratio. The extract was introduced dropwise into the $AgNO_3$ solution while maintaining continuous stirring on a hot plate at a controlled temperature of 37 °C. The reaction mixture was stirred for 24 hours to ensure the thorough reduction of silver ions. A distinct color transition from pale brown to dark brown primarily confirmed the successful formation of MdSE mediated Ag/AgCl nanoparticles (MdSE-Ag/AgCl-NPs). Post-synthesis, the mixture was subjected to centrifugation at 10 000 rpm for 30 minutes to separate the nanoparticles. The obtained nanoparticles were then washed three times with deionized water to remove any residual impurities and unbound compounds. Finally, the nanoparticles were dried in an oven at 40 °C for 24 hours to obtain a consistent powdered form and kept at 4 °C for characterization and antibacterial experiments.

Characterization of MdSE-Ag/AgCl-NPs

Ultraviolet-visible spectroscopy (UV-vis). The optical properties and formation of MdSE-Ag/AgCl-NPs were confirmed using UV-visible spectrophotometer. The absorbance spectra from the resulting MdSE-Ag/AgCl-NPs reaction mixture were recorded using the SpectraMax ID3 Multi-Mode Microplate Reader (USA) within the wavelength range of 300–700 nm and at 1 nm resolution, with deionised water serving as the blank.

Dynamic light scattering (DLS) and zeta potential. The hydrodynamic size and polydispersity index (PDI) of the phytofabricated MdSE-Ag/AgCl-NPs were evaluated using the DLS technique operated in Zetasizer Nano-ZS (Malvern Instruments, UK). The resulting MdSE-Ag/AgCl nanoparticles were redispersed in deionized water and sonicated for 5 minutes at 25 °C to achieve a uniform suspension. Measurements were conducted at 25 °C with a scattering angle of 90°. The zeta potential (ξ) was assessed using an electrophoretic cell with the same Zetasizer instrument to determine the surface charge, which reflects the stability of the nanoparticle suspension. Each measurement was performed in triplicate to ensure the reliability and reproducibility of the results.

Fourier-transform infrared spectroscopy (FTIR). FTIR was utilized to analyze the functional groups present in MdSE and comparing it to the spectrum produced with MdSE-Ag/AgCl-NPs. This is to identify the biomolecules associated with the silver and bound to the surface atoms of the nanoparticles, acting as capping agents. Spectral analysis was performed using an FTIR spectrometer (Agilent Cary 630 FTIR, USA) within a scanning range of 4000–640 cm^{-1}.

Field emission scanning electron microscopy (FESEM). The size and surface morphology of the synthesized MdSE-Ag/AgCl-NPs were examined using a FESEM (JSM-7600F, JEOL, Tokyo, Japan). Imaging was conducted at an accelerating voltage of 5 kV, with a working distance of 4.4 mm, and magnifications ranging from 50 000× to 100 000×. Prior to FESEM observation, the MdSE-Ag/AgCl-NPs powder was carefully mounted onto a tubular aluminum stub using double-sided adhesive tape. The sample was then sputter-coated with a thin platinum layer using a JEOL JEC-3000FC auto fine coater, to strengthen their conductivity and for high quality imaging.

X-ray diffraction (XRD). X-ray diffractograms of the samples were recorded within the 2θ range of 20–90° using a Rigaku SmartLab diffractometer (Rigaku Corporation, Tokyo, Japan). The instrument was operated at 40 kV accelerating voltage, 30 mA current, monochromatic CuKα radiation with a wavelength of 1.54059 Å, a scan rate of 3°/minute, and a parallel beam configuration in $2\theta/\theta$ scan mode. The acquired diffractograms were analyzed using SmartLab Studio II (version 4.4.241.0, Rigaku Corporation, Tokyo, Japan). Phase identification was performed by comparing the diffraction patterns with reference data from the ICSD (Inorganic Crystal Structure Database). The crystallite size of the nanoparticles was determined using the Debye–Scherrer equation, eqn (1):

$$D = \frac{(K \times \lambda)}{(\beta \times \cos\theta)} \quad (1)$$

where D denotes the average crystallite size, K is the Scherrer constant (0.94), λ represents the wavelength (1.54059 Å), β corresponds to the full width at half maximum (FWHM), and θ is the Bragg angle.

High resolution field emission transmission electron microscopy (HR-FETEM). The synthesized MdSE-Ag/AgCl nanoparticles were characterized using high-resolution FETEM (JEOL JEM-2100F, Tokyo, Japan), which was equipped with a selected area electron diffraction (SAED) attachment and operated at an accelerating voltage of 200 kV. This technique facilitated the examination of the nanoparticle's morphology, size, and SAED patterns. The lattice distances observed in the FETEM micrographs were analyzed using Gatan Digital Micrograph software.

For sample preparation, MdSE-Ag/AgCl-NPs powders were dispersed ultrasonically in ethanol, after which a drop of the resulting suspension was deposited onto a carbon coated copper grid using a micropipette. The solvent was then allowed to evaporate.

Energy-dispersive X-ray (EDX). Elemental identification was performed with an energy-dispersive X-ray detector (X-Max, Oxford Instruments, UK) integrated into the HR-FETEM system. The elemental composition and chemical status of the sample were acquired and processed using Aztec software (version 3.1, Oxford Instruments, UK).

Antibacterial activity

Bacterial strains. The bacterial strains used in this study were sourced from the American Type Culture Collection (ATCC, Rockville, Maryland, United States). The pathogenic bacterial strains evaluated for the antibacterial activity were the Gram-negative bacterial strains namely *E. coli* (ATCC 25922) and *P. aeruginosa* (ATCC 27853), while the Gram-positive strain includes *S. aureus* (ATCC 25923). Prior to analysis, all bacterial strains were streaked onto blood agar plates (Thermo Scientific Microbiology Sdn. Bhd., Malaysia) to verify their pathogenic virulence. The presence of a haemolytic zone confirmed their viability and pathogenicity before proceeding with further testings.

Inoculum preparation. Bacterial strains were initially cultured on tryptic soy agar (TSA, Oxoid, Hampshire, England) plates and incubated at 37 °C for 24 hours to facilitate bacterial growth. The bacterial cultures were prepared in accordance with the guidelines established by the Clinical and Laboratory Standards Institute (CLSI) (2018).[27] Individual colonies were solubilized into 20 mL of tryptic soy broth (TSB, Oxoid, Hampshire, England) and incubated under the same conditions for 24 hours to ensure bacterial proliferation. Following incubation, the bacterial suspensions were diluted in 10 mL of TSB, with the turbidity adjusted to a final concentration of 10^6–10^8 CFU mL^{-1} against 0.5 index of the McFarland standard, which were then tested with varied treatments.

Minimum inhibitory concentration (MIC) and minimum bactericidal concentration (MBC). The broth microdilution assay, as recommended by the CLSI (2018),[27] was employed to determine the minimum inhibitory concentration (MIC) of MdSE-Ag/AgCl-NPs against the tested bacterial strains using a 96-well microtiter plate.

To prepare the bacterial inoculum, overnight bacterial cultures were adjusted to a 0.5 McFarland standard, corresponding to approximately 10^6–10^8 CFU mL^{-1}. For the assay setup, 200 μL of TSB medium was added to the first column, serving as the negative growth control (devoid of nanoparticles and bacteria), while the second column was designated as the positive growth control, containing 200 μL of bacterial suspension. From the third to the twelfth wells, 100 μL of TSB was distributed into each well. Next, 100 μL of the synthesized MdSE-Ag/AgCl nanoparticles suspension (at the highest concentration) was introduced into the third well. A serial twofold dilution was then performed by transferring 100 μL from the third well to the fourth well, continuing this process sequentially until reaching the twelfth well. Subsequently, 100 μL of the bacterial suspension was added from the third to the twelfth wells. Alongside the nanoparticles, gentamicin antibiotic (as a positive standard control), Medjool date seeds extract (MdSE), and $AgNO_3$ solution were included for comparison and tested under identical procedures. After thorough mixing, the microtiter plates were covered with lids and incubated at 37 °C for 24 hours. The test was carried out in triplicates. The MIC was defined as the lowest concentration at which no visible bacterial growth was observed, as compared to the positive and negative growth controls.[28]

To determine the minimum bactericidal concentration (MBC), 10 μL of the bacterial suspension from each well was transferred onto TSA plates. Samples from the negative and positive growth control were also inoculated onto the agar. The TSA plates were then incubated at 37 °C for 24 hours, after which the MBC was recorded. The MBC value was defined as the lowest concentration of the test compound that completely inhibited bacterial growth on TSA after incubation.[29]

Tolerance level. The tolerance of the tested bacterial strains toward MdSE-Ag/AgCl-NPs, gentamycin, MdSE, and $AgNO_3$ was evaluated following the approach outlined by Dash *et al.* (2020),[30] utilizing their MIC and MBC values. A tolerance value of 16 or higher indicates a bacteriostatic effect, while a value of 4 or lower is classified as bactericidal. The following eqn (2) was used:

$$\text{Tolerance level} = \frac{\text{MBC}}{\text{MIC}} \tag{2}$$

***In vitro* biofilm inhibition assay.** The anti-biofilm potential of the synthesized MdSE-Ag/AgCl-NPs was assessed using a 96-well microtiter plate assay conducted under aseptic conditions, following a previously described method with slight modifications.[31–33] To initiate the assay, 200 μL of fresh bacterial suspension (0.5 McFarland) prepared in TSB, containing varying concentrations (1/4, 1/2, 1, 2, and 4*MIC) of MdSE-Ag/AgCl-NPs, was dispensed into designated wells of the microtiter plate. The plate was then incubated at 37 °C for 24 hours to allow biofilm formation.

After incubation, the well contents were discarded by inverting and gently tapping the plate. To remove non-adherent bacteria, 200 μL of deionized water was added to each well, followed by three consecutive washes. The plate was then dried at 60 °C, after which 200 μL of 0.1% (v/v) crystal violet solution was introduced into each well to stain the adhered biofilm. After a 30 minutes incubation, excess dye was discarded, and the wells were rinsed three times with deionized water to eliminate residual stain. To solubilize the bound crystal violet, 200 μL of 95% ethanol was added to each well, and the plate was gently agitated for 5 minutes. The optical density (OD) of the stained biofilms was measured at 570 nm using a microplate reader (SpectraMax ID3 Multi-Mode Microplate Reader, USA). Wells containing sterile TSB alone served as the negative growth control, while those containing only bacterial suspensions functioned as positive growth control. Additionally, gentamicin (positive standard control) and MdSE were tested under the same conditions for comparison. The biofilm inhibition percentage (%) was calculated using the formula, eqn (3):

$$\%\ \text{Biofilm inhibition} = \left[1 - \frac{\text{OD(T)}}{\text{OD(PGC)}}\right] \times 100 \tag{3}$$

where OD(PGC) represents the absorbance of the positive growth control-stained biofilm and OD(T) corresponds to the absorbance recorded for different sample treatments (MdSE-Ag/AgCl-NPs, gentamicin, and MdSE). All the experiments were conducted in duplicate and results were reported as mean ± standard deviation (SD). Statistical analysis was performed

using SPSS software (version 29.0.0.0), employing one-way ANOVA, with $p < 0.05$ considered statistically significant.

Results and discussion

Characterization of MdSE-Ag/AgCl-NPs

Optical analysis (MdSE-Ag/AgCl-NPs synthesis and UV-vis analysis). The initial indication of MdSE-Ag/AgCl nanoparticle synthesis was visually observed through a distinct colour change in the reaction mixture, from pale brown to dark brown, upon the addition of 1 mg mL^{-1} MdSE to 1 mM $AgNO_3$ solution (Fig. 1). This visual shift suggested the reduction of Ag^+ ions and the formation of silver nanoparticles, a phenomenon commonly associated with the excitation of surface plasmon vibrations on the nanoparticle surface.

UV-vis spectrophotometric analysis further confirmed nanoparticles formation, where a strong and well-defined absorption peak appeared at 450 nm (Fig. 2), consistent with the surface plasmon resonance (SPR) characteristic of silver nanoparticles. The appearance of this peak falls within the expected SPR range for AgNPs (typically 410–455 nm),[34] and is indicative of spherical nanoparticle morphology and successful bioreduction of silver ions.[35] This finding aligns well with the previous reports on phytofabricated AgNPs synthesized using date fruit extracts and saponins derived from Ajwa date seeds, which demonstrated a closely related SPR peak at approximately 440 nm.[36,37] This optical feature results from the collective oscillation of conduction electrons stimulated by incident light, and its position can be influenced by factors such as particle size, shape, and dielectric environment. The absorption at 450 nm observed in this study tallies closely with reports from similar green synthesis approaches, validating the formation of phytofabricated MdSE-Ag/AgCl nanostructures, with bioactive components in the Medjool extract likely acting as both reducing and stabilizing agents during nanoparticle nucleation and growth.

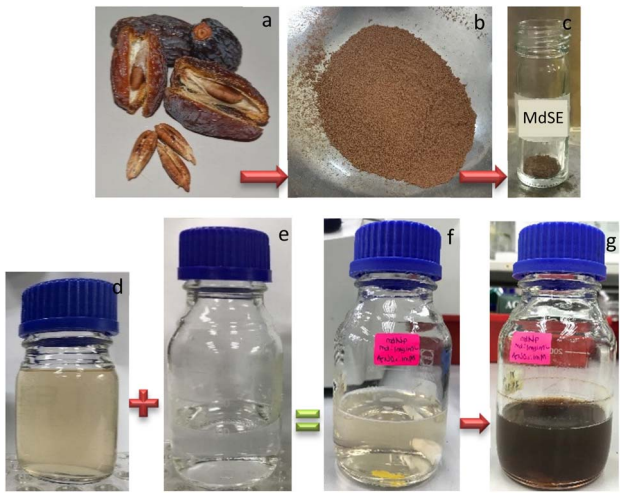

Fig. 1 Visual representation of the phytofabrication process of silver nanoparticles using Medjool date seeds extract (MdSE). (a) Medjool date seeds, (b) seeds ground into fine powder and, (c) ultrasonicated extract obtained in the form of powder. Formation of MdSE-Ag/AgCl nanoparticles indicated by a visible colour change from (f) pale brown mixture to (g) dark brown upon the addition of (d) ethanolic MdSE at 1 mg mL^{-1} to (e) 1 mM $AgNO_3$.

Dynamic light scattering (DLS) and zeta potential. To assess the hydrodynamic size and dispersion behavior of the phytofabricated MdSE-Ag/AgCl nanoparticles, DLS analysis was performed. The particles exhibited a Z-average diameter of 168.5 nm and a PDI of 0.207 (Fig. 3a), reflecting a moderately uniform size distribution and minimal aggregation in suspension. These findings suggest that the phytofabricated nanoparticles possess a stable colloidal profile suitable for biological applications. The relatively larger size detected by DLS, in contrast to the smaller diameters observed *via* FESEM and FETEM imaging in many reports, can be attributed to the measurement of hydrodynamic diameter, which accounts for the core nanoparticle along with surface-bound biomolecules, hydration layers, surface electrical layers, capping agents derived from MdSE, and any loosely bound stabilizing layers.[38,39] This discrepancy is commonly observed in green-synthesized nanoparticles.[35,40] Comparable findings were reported by Khader *et al.* (2022)[24] and Zaheer (2018),[37] where AgNPs synthesized from date seeds and fruit extracts showed a DLS size of 203 nm and predominantly 100–200 nm, respectively, while electron microscopy shows substantially smaller particle sizes in dry state. Furthermore, zeta potential analysis revealed a value of −36.3 mV (Fig. 3b). This confirms the strong surface charge and electrostatic repulsion among particles, likely the result of adsorbed free nitrate ions or negatively charged phytochemicals, contributing to long-term colloidal stability and minimizing agglomeration.

Fourier-transform infrared spectroscopy (FTIR). FTIR spectroscopy is a commonly used, rapid, reliable, and cost-effective analytical tool for identifying functional groups present in Medjool date seeds extract that contribute to the reduction, capping, and stabilization of phytofabricated MdSE-Ag/AgCl nanoparticles. A comparative evaluation in the appearance and shifts of absorption peaks (Fig. 4a and b), identifies the involvement of various phytochemical constituents, detected through molecular vibration, such as stretching and bending within the infrared region (4000–640 cm^{-1}). Literature review detailing date seeds and fruit extracts were referred to confirm the profile of the FTIR peaks obtained (Table 1).

In the MdSE spectrum, a broad peak at 3425 cm^{-1} corresponds to O–H stretching which suggest the occurrence of surface adsorbed alcohols (carbohydrates such as isomaltose) and polyphenols (flavonoids and phenolic acid), which shifted to 3444 cm^{-1} in the nanoparticle spectrum, suggesting hydrogen bonding interactions and its involvement in surface binding. The weak C–H stretching vibration near 2995 and 2912 cm^{-1} were retained in both spectra, likely to be originating from aliphatic hydrocarbons (probably sugars) present in the extract.

A prominent shift was observed at 1647 cm^{-1} (MdSE) to 1662 cm^{-1} (MdSE-Ag/AgCl-NPs), typically associated with C=C stretching in alkene groups (flavonoid), N–H amide stretch corresponding to the protein retrieved from the seed extract or

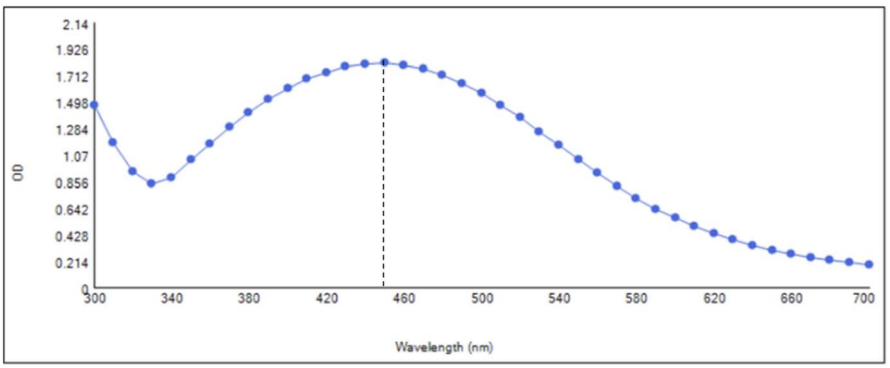

Fig. 2 The UV-vis absorption spectrum of silver nanoparticle solution synthesized from the ethanolic extract of *P. dactylifera* Medjool date seeds (MdSE).

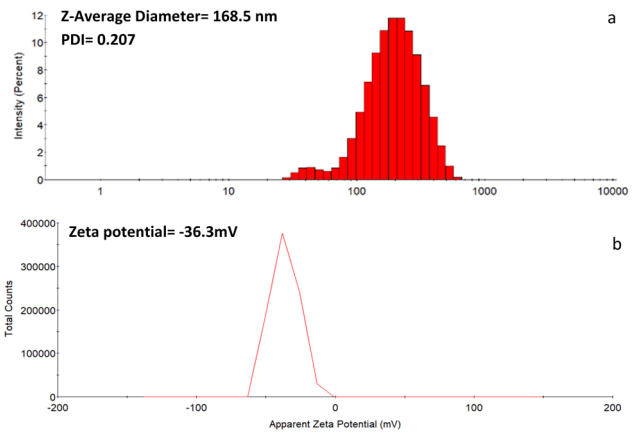

Fig. 3 Spectra of (a) particle size distribution, PDI, and (b) zeta potential of phytofabricated silver nanoparticles (MdSE-Ag/AgCl-NPs).

C═O carbonyl stretching commonly associated with biomolecules responsible for metal ion reduction and preventing particle accumulation.[41] Apart from being found in ketones, aldehyde and carboxylic acids, carbonyl stretching vibration could also possibly arises from the amide linkage within protein.[42] Such observations also suggest the presence and binding of proteins with AgNPs which may be involved in the process of their formation and stabilization. The peak at 1436 cm^{-1} represents bending vibration of C–H bond in methylene hydrocarbon while peaks near 1309 and 1016 were attributed to the C–O stretching vibration of possible alcohols of polysaccharides, flavones (flavonoids), ethers, esters, carboxylic acids, glycosides, or anhydrides coating the surface of the nanoparticle.[36,43] Additional bands between 951 – 668 cm^{-1} further support the existence of alkene stretchings.[23] Notably, new or shifted bands appearing below 700 cm^{-1}, such as at 697 and 668 cm^{-1}, may indicate halo-alkane stretch or metal-chloride vibrations,[44] suggesting for successful coordination with silver ions.

Thus, these spectral variations affirms that various functional groups namely O–H group of polyphenols, amide group of proteins, carbonyl possessing compounds, C–O possessing groups, carbohydrates, and chlorides have adsorbed to the surface of the silver nanoparticles or involved in the reduction of Ag^{+} to Ag^{0} nanoparticles. This supports the effectiveness of the Medjool seeds extract in the green synthesis of MdSE-Ag/AgCl nanoparticles with stable organic surface coatings.

Field emission scanning electron microscopy (FESEM). FESEM operates by emitting electrons that are accelerated under a strong electric field, enabling high-resolution imaging of nanoscale surface topographies. In this study, FESEM was used to investigate the morphology and size distribution of the phytofabricated MdSE-Ag/AgCl nanoparticles. The micrograph (Fig. 5a) disclosed the predominantly spherical nature of the synthesized nanoparticles exhibiting moderate agglomeration, a phenomenon often attributed to the high surface energy of nanoscale materials and drying effects during sample preparation. Particle size measurements calculated with the ImageJ software revealed an average diameter of 28.10 ± 5.1 nm and a size distribution ranging from 16.56 nm to 43.76 nm (Fig. 5b), indicating moderate polydispersity. The size of synthesized MdSE-Ag/AgCl-NPs falls within the acceptable nanoscale limit range, thus, suggesting successful synthesis of relatively small-sized silver nanoparticles. In contrast, SEM analysis in studies by Aldayel *et al.* (2021)[43] and Abdel-Alim *et al.* (2023)[48] reported broader and larger size distributions for silver nanoparticles synthesized from Ajwa, Iklas, and Shishi date seeds, with size ranging from 15–80 nm, 46.79–73.72 nm, and 527–776 nm, respectively. Despite the visible aggregation, the particle size and well-defined individual spherical shape were still visible in Fig. 5a, indicating a relatively uniform distribution. This could be associated to the role of the capping agents from MdSE that provides stability and preventing the nanoparticles from agglomerating into a macro fused particle with an unidentifiable shape.

Arshad *et al.* (2021)[49] and Acharya *et al.* (2018)[50] have emphasised that both the nanoparticle shape and size are critical determinants in nanoparticle therapeutic performances. Small sized and spherical nanoparticles, as observed in this study, were expected to penetrate pathogenic microbial membranes more efficiently and are able to generate significant damage to bacterial cells due to the larger specific surface area resulting from their spherical geometry, especially when compared to nanorod and nanowire structures.

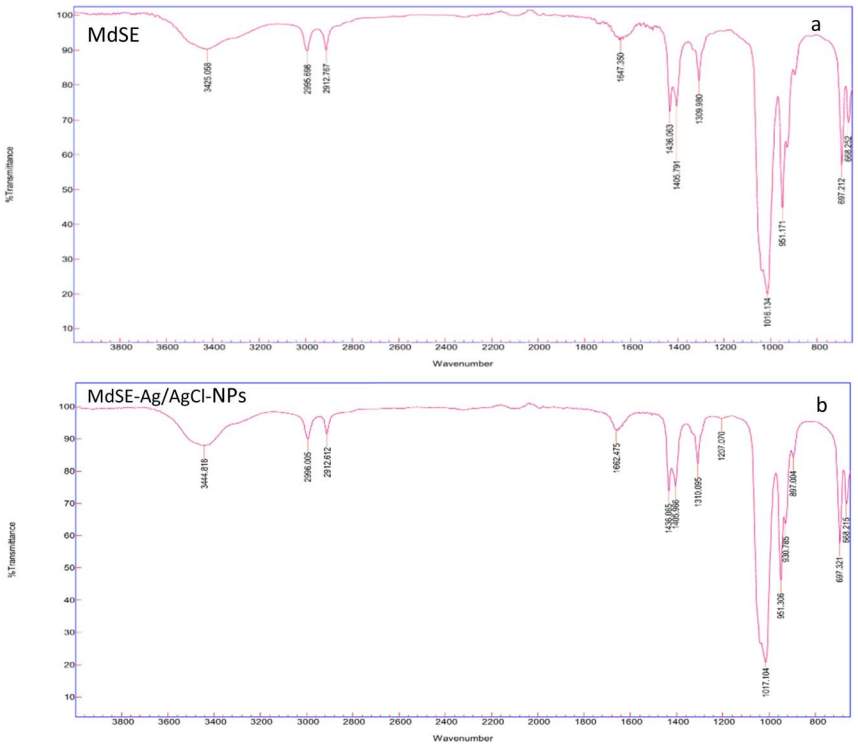

Fig. 4 FTIR spectra recorded from (a) MdSE and (b) phytofabricated MdSE-Ag/AgCl-NPs, revealing peaks of functional groups involved.

X-ray diffraction (XRD). The crystalline nature of the dry MdSE-Ag/AgCl nanoparticles was elucidated through the spectrum obtained from XRD analysis, conducted across a 2θ scanning range of 20–90°, as shown in Fig. 6. A focused monochromatic X-ray beam was directed at the powdered sample, producing various diffraction patterns that were interpreted using Bragg's equation to reveal the crystalline characteristics of the nanoparticles. Prominent diffraction peaks were observed at 2θ values of 38.12°, 44.26°, 64.48°, 77.46°, and 81.48°, corresponding to the (111), (200), (220), (311), and (222) crystallographic reflection planes of metallic silver, Ag (ICSD reference code: 01-080-4432). Additionally, five more diffraction peaks appeared as a result of Bragg's reflection at 27.84°, 32.26°, 46.29°, 54.84°, and 57.53°, attributed to the (111), (200), (220), (311), and (222) planes of the silver chloride, AgCl phase (ICSD reference code: 00-001-1013). The XRD reflections associated with these lattice planes confirm the formation of face-centered cubic (fcc) crystalline structures for both Ag and AgCl nanoparticles, consistent with the standard ICSD database (DB). The 2θ values and planes reported in this study closely match to those previously observed for Ag/AgCl nanoparticles synthesized using *Origanum ehrenbergii*,[10] further assuring the coexistence of silver and silver chloride entities.

Most of the diffraction peaks appeared intense and narrow, revealing the highly crystalline structure of the MdSE-Ag/AgCl nanoparticles synthesized, particularly those corresponding to silver. The sharp and greater intensity of Ag-related reflection at 111 plane compared to those of AgCl suggests the

Table 1 FTIR analysis and probable functional group associated to MdSE-Ag/AgCl nanoparticles

IR peak position (cm^{-1})		
MdSE	MdSE-Ag/AgCl	Functional group(s)
3425	3444	O–H stretch[24]
2995	2996	C–H stretch[23]
2912	2912	C–H stretch[23,24]
1647	1662	C=C stretch/N–H amide stretch/C=O stretch[25,45,46]
1436	1436	C–H bending[45]
1309	1310	C–O stretch[47]
1016	1017	C–O stretch[43]
951	951	C=C stretch[23,48]
697	697	C–X stretch overlapping with chloride/C=C stretch[23,24,43]
668	668	C–X stretch overlapping with chloride/C=C stretch[23,24,43]

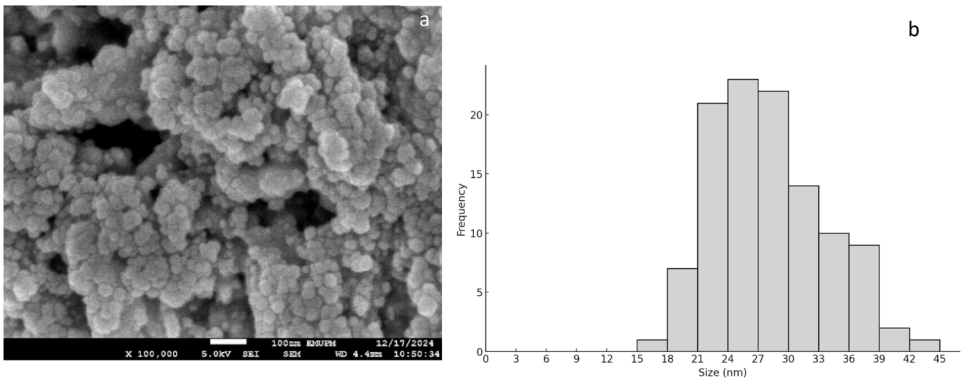

Fig. 5 (a) Field emission scanning electron microscopy (FESEM) image detailing surface morphology of the synthesized MdSE-Ag/AgCl nanoparticles and (b) histogram showing size distributions of the nanoparticles.

predominance of silver nanoparticles in the sample. Crystallite sizes for Ag and AgCl were calculated using the Scherrer equation, yielding approximate sizes of 16.67 nm and 12.41 nm, respectively, with a lattice parameter measured at 4.08601 Å. These results demonstrate that the phytofabrication method employed not only enabled the successful formation of AgNPs but also facilitated the concurrent generation of AgCl nanostructures. This dual formation is likely driven by the presence of chloride ions in the Medjool date seeds extract, which potentially interacted with Ag^+ ions from $AgNO_3$ during synthesis, leading to AgCl formation. Interestingly, this is the first report detailing the concurrent formation of AgCl nanoparticles alongside Ag, deriving from date seeds extract, particularly of Medjool variant. Furthermore, this work uniquely reports a complete set of silver diffraction planes in a single diffractogram, reflecting an extended crystalline silver planes (311 or 222) compared to previous reports on date seeds and fruit-mediated silver nanoparticle synthesis.[24,25,42,51]

High resolution field emission transmission electron microscopy (HR-FETEM). Detailed analysis on the morphology and size distribution of the MdSE-Ag/AgCl nanoparticles were performed employing HR-FETEM. TEM is widely regarded as one of the most suitable techniques for determining the average size of nanoparticles, as it provides clear visualization of their crystalline structure. Analysis of the synthesized Ag/AgCl nanoparticles revealed a narrow size distribution, indicating that the particles were relatively small and within an acceptable nanosize range (Fig. 7). A histogram reflecting particle size distribution was generated by analyzing over 150 particles using ImageJ software (Fig. 7d). Based on the measurements, the nanoparticles displayed a polydisperse profile with no agglomeration and a predominantly spherical morphology (Fig. 7a and b). The particle sizes ranged from 6.23 to 38.01 nm, with an average size of 16.75 ± 7.25 nm, close to the crystallite size calculated from the XRD analysis. The observed decrease in the average diameter of the phytofabricated MdSE-Ag/AgCl-NPs likely results from a reduced presence of larger particles and a greater proportion of smaller-sized nanoparticles within the distribution. Such narrow polydispersity may be influenced by the diverse array of phytochemical constituents present in the extract, each contributing differently to the reduction and stabilization process. The HR-FETEM observations on the MdSE-Ag/AgCl nanoparticles are consistent with the findings reported in several previous studies, where an almost similar size ranges and spherical morphologies were obtained. For instance, silver nanoparticles synthesized from date pits[25] exhibited sizes between 1–40 nm, while those originating from date fruits[37] ranged from 3–30 nm. Similarly, AgNPs synthesized using *Cassia occidentalis* L. seeds extract were reported between 6.44–28.50 nm.[52] On the contrary, various other ranges, broader,

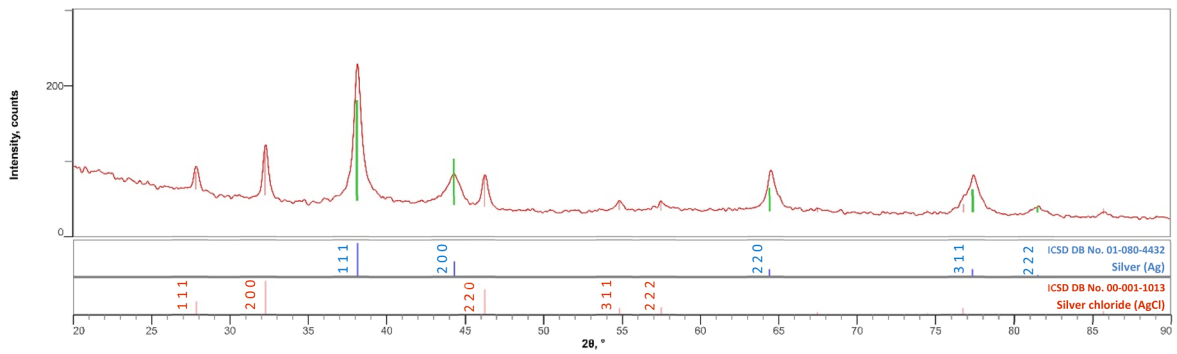

Fig. 6 X-ray diffraction patterns of Ag-NPs and AgCl-NPs phytofabricated from MDSE.

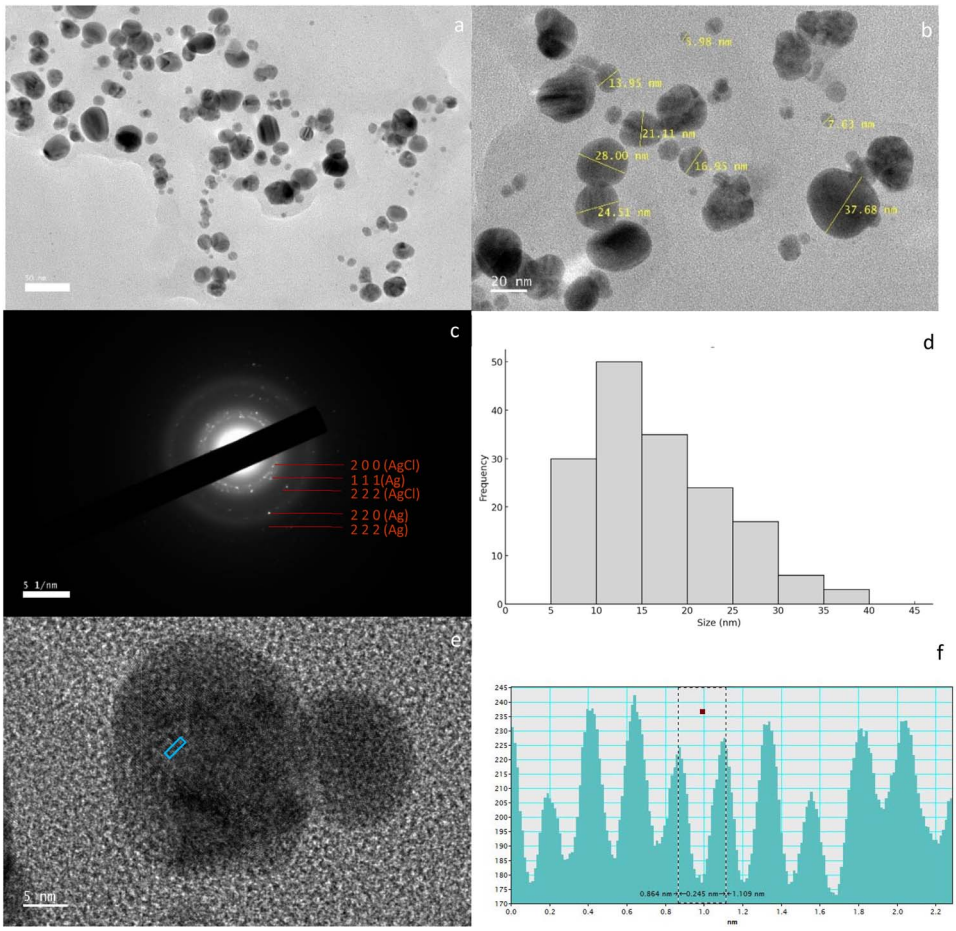

Fig. 7 High resolution field emission transmission electron microscope (HR-FETEM) images of phytofabricated MdSE-Ag/AgCl-NPs at a scale bar of (a) 50 nm (50 000×), (b) 20 nm (100 000×), (c) selected area electron diffraction patterns (SAED), (d) particle size distribution histogram, and (e and f) high-resolution image of single nanocrystal showing lattice fringes with a spacing of 0.245 nm at 500 000×.

and larger size distribution were documented, namely AgNPs derived from Ajwa date seeds (15–80 nm),[23] date fruit (20–100 nm),[46] and a relatively narrower range (1–10 nm) from saponin-derived silver nanostructures from dates, due to the use of a single purified compound.[36] These comparisons highlight the efficiency of the Medjool seeds extract in producing small and well-dispersed nanoparticles.

Further structural characterization utilizing crystallographic technique was performed using selected area electron diffraction (SAED) during HR-FETEM analysis. The SAED patterns exhibited distinct pattern of concentric rings formed by a set of point reflections, showing a polycrystalline nature of the MdSE-Ag/AgCl-NPs material (Fig. 7c). These rings corresponded to Bragg diffraction and revealed a set of lattice planes consistent with those of the Ag phase specifically at (111), (220), and (222), as well as the (200) and (222) planes attributed to the AgCl phase. The indexing of these reflections confirmed a face-centered cubic structure for the polycrystalline Ag/AgCl nanoparticles, in full agreement with the XRD findings. Additionally, the HR-FETEM analysis revealed lattice fringes (Fig. 7e) of a single nanocrystal and an interplanar spacing of 2.45 Å (0.245 nm) (Fig. 7f), corresponding closely with the (111) plane of metallic silver which is the most intense reflection observed in the XRD spectrum.

Energy-dispersive X-ray (EDX). The elemental composition of phytofabricated MdSE-Ag/AgCl nanoparticles was investigated and confirmed by the semi-quantitative analysis utilizing EDX spectroscopy. Copper substrate was used for mounting, the contribution of which was not taken into account in the calculations. The EDX spectrum exhibited a strong signal peak at 3 keV (Fig. 8), revealing the major presence of silver, which aligns with the typical optical absorption peak of metallic silver nanocrystallites due to surface plasmon resonance.[53] Given that silver is the primary material targeted, the spectrum also revealed the presence of chloride peaks at 2.7 keV, confirming the successful synthesis and co-existence of metallic MdSE-Ag-NPs with MdSE-AgCl-NPs as nanohybrids, and this outcome corroborate to the reports of Ag/AgCl synthesized from *Oedera genistifolia* and *Momordica charantia*.[16,54]

Quantitative analysis proves the successful formation of MdSE-Ag/AgCl nanoparticles and showed its predominant elements to be silver with a weight percentage of 73.22%, followed by carbon (18.20%), chlorine and oxygen (3.03%), silicon (2.30%), and sodium (0.21), which are in line with those

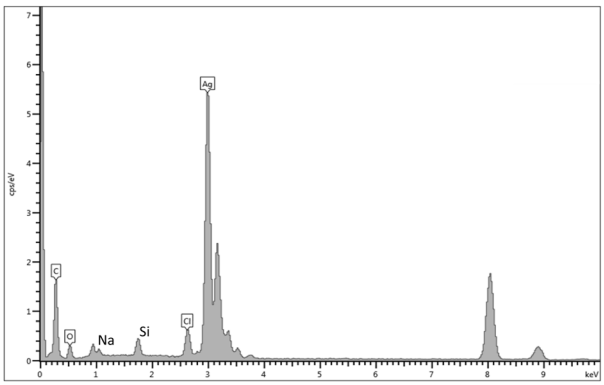

Fig. 8 EDX spectrum of MdSE-Ag/AgCl-NPs.

reported by Stozhko *et al.* (2024)[55] and Yassin *et al.* (2022)[56] (Table 2). The prominent silver signal validates the effective reduction of Ag^+ ions to elemental silver, while the presence of other elemental peaks could have originated from the organic shell surrounding the silver nucleus, as described by Stozhko *et al.* (2024).[55] This shell likely attributed to the biomolecules and organic compounds (carbohydrates and proteins) derived from MdSE extract, which could have also functioned as natural capping and stabilizing agents during silver nanoparticles synthesis as suggested by Maryani and Septama (2022).[57] The detection of chloride ions (Cl^-), naturally occurring macronutrients in plants, are known to play essential roles in regulating photosynthesis and maintaining homeostasis in plants.[58] Furthermore, the presence of sodium likely reflects its diffusion from the extract into the silver nanoparticles owing to their small ionic radius and high diffusion coefficient, a phenomenon commonly observed in biosynthesized metallic and metal oxide nanomaterials.[32,59] The detection of silicon in current EDX spectrum are supported with the findings from Allemailem *et al.* (2022),[23] who have reported the presence of carbon, oxygen, sodium, and silicon in AgNPs synthesized from Ajwa date seeds extracts. However, the carbon signal observed in the spectrum may also have originated from the carbon coating on the copper grid used for sample mounting. This corroborates the idea that the other elemental contributions originate from the Medjool seeds extract used in this study.

Antibacterial activity

MIC and MBC. The antimicrobial potential of biosynthesized MdSE-Ag/AgCl-NPs, gentamycin, MdSE, and $AgNO_3$ were assessed using the broth microdilution method, against *E. coli*, *P. aeruginosa*, and *S. aureus* as tabulated in Table 3. The MdSE-Ag/AgCl nanoparticles showed superior antibacterial activity, by demonstrating lower MIC values against all tested bacterial strains at 0.039 mg mL^{-1} for *E. coli* and 0.078 mg mL^{-1} for *P. aeruginosa* and *S. aureus*. The MBC values were recorded at either 0.078 mg mL^{-1} (*E. coli*) or 0.156 mg mL^{-1} (*P. aeruginosa* and *S. aureus*). Among the strains, *E. coli* exhibited the greatest susceptibility, showing the lowest MIC and MBC (0.039 mg mL^{-1} and 0.078 mg mL^{-1}). This value corresponds to a previously reported AgNPs synthesized from date seed variant of Iklas, that scored an MIC value at 32.6 μg mL^{-1}.[43]

Additionally, the values recorded in this study are considerably more effective when compared with previously reported green-synthesized AgNPs. For example, AgNPs synthesized using *Trigonella foenum-graecum* seeds extract exhibited an MIC of 125 μg mL^{-1} against *E. coli*,[60] while those derived from *Ephedra gerardiana* and *Annona reticulata* showed MICs of 125 μg mL^{-1} and 62.5 μg mL^{-1}, respectively.[61,62] Adding to this, phytochemically derived Ag/AgCl nanoparticles from *O. ehrenbergii* reported an MIC of 62.5 μg mL^{-1} against *E. coli*, further highlighting the superior potency of the MdSE-Ag/AgCl nanoparticles developed in the present study.[10] In the case of *P. aeruginosa*, *Pteris vittata*-mediated AgNPs were reported to have an MIC of 100 μg mL^{-1},[63] whereas *Moringa oleifera*-based AgNPs exhibited an even higher MIC of 250 μg mL^{-1}.[64] Similarly, against *S. aureus*, AgNPs from *Priva cordifolia* and Ag/AgCl-NPs from *O. genistifolia* required 100 μg mL^{-1} and as high as 500 μg mL^{-1} to inhibit growth, respectively.[16,65] In addition, the MBC values obtained against all tested bacterial strains were substantially lower than the Ag/AgCl nanoparticles reported by Hachem *et al.* (2024), that required a concentrations of ≥1 mg mL^{-1} to completely kill the bacteria.[10] The MIC and MBC values retrieved in the current study are also notably lower than those of the crude MdSE, which required much higher concentrations (MICs: 3.125–12.5 mg mL^{-1}; MBCs: 25 mg mL^{-1}) to achieve bacterial inhibition and complete eradication. The enhanced performance of the phytofabricated nanoparticles over the extract can be attributed to the well-established synergistic interaction between silver ions and phytochemicals derived from plant matrices.[66] This reinforces their broad-spectrum antibacterial efficacy and the potential advantage of using Medjool date seeds extract as a reducing and stabilizing agent

Table 2 Quantitative results obtained from elemental analysis of MdSE-Ag/AgCl-NPs

Element	Wt (%)
Ag	73.22
C	18.20
Cl	3.03
O	3.03
Si	2.30
Na	0.21

Table 3 Determination of MIC and MBC values (mg mL^{-1}) for various treatments against selected microbial pathogens

	E. coli (ATCC 25922)		*P. aeruginosa* (ATCC 27853)		*S. aureus* (ATCC 25923)	
Treatments	MIC	MBC	MIC	MBC	MIC	MBC
MdSE[a]	12.5	25.0	6.25	25.0	3.125	25.0
MdSE-Ag/AgCl-NPs[a]	0.039	0.078	0.078	0.156	0.078	0.156
Gentamicin[a]	0.010	0.039	0.010	0.020	0.010	0.020
$AgNO_3$[a]	0.039	0.039	0.039	0.078	0.156	0.312

[a] The concentration of the treatments are in mg mL^{-1}.

for nanoparticle biosynthesis. Gentamicin, on the other hand, exhibited much lower MIC and MBC values for all bacterial strains, thereby validating the experiment.

$AgNO_3$ exhibited an MIC of 0.039 mg mL^{-1} for Gram-negative bacteria and 0.156 mg mL^{-1} for *S. aureus*, confirming its strong antimicrobial action. Although both $AgNO_3$ and plant-mediated silver nanoparticles exhibit cytotoxic properties, $AgNO_3$ is known to display significantly higher cytotoxicity, particularly at higher concentrations.[67] Its application is often limited clinically when compared to biogenically synthesized silver nanoparticles. In contrast, biosynthesized AgNPs like MdSE-Ag/AgCl-NPs offer improved safety and stability, aligning with the principles of green nanotechnology.

The underlying working mechanism of silver nanoparticles lies in their ability to disrupt bacterial function at multiple simultaneous targets, thereby reducing the likelihood of bacteria developing resistance to AgNPs. These targets include their interactions with the bacterial cell membrane, cell wall, intracellular proteins, lipopolysaccharides (LPS), nucleic acids, and metabolic enzymes inhibition (FOF1-ATPase) in charge of bacterial growth and reproduction.[68] Eventually, these interference to metabolic pathways and intracellular changes, elevates oxidative stress, membrane disintegration, and ultimately, cell death. Supporting this, SEM observations of *E. coli* and *S. aureus* treated with silver nanoparticles revealed morphological surface distortions compared to the control cells, illustrating a contact-action mechanism in which proposes the capability of AgNPs adsorbing to the bacterial cytoderm, penetrating the cytomembrane, and triggering apoptosis.[69]

It is worth pointing that several physicochemical factors influence the antimicrobial performance of AgNPs, particularly particle size, shape, surface charge, and concentration.[70] These parameters appear to correlate with the outcomes of the present study, in which spherical MdSE-Ag/AgCl nanoparticles with an average diameter of 16.75 nm was produced. Among the various nanoparticle morphologies (spherical, disk-shaped, and triangular plate), previous studies have shown that spherical nanoparticles exhibit superior antibacterial activity, largely due to their enhanced silver ion release, which intensifies interactions with planktonic bacterial cells and accelerates bacterial killing.[71] Furthermore, the nanoscale size of the MdSE-Ag/AgCl-NPs may enhance their ability to traverse bacterial membranes, facilitating intracellular entry, and inflicting irreversible cellular damage. A similar size-dependent mechanism was proposed by Loo *et al.* (2018),[72] who suggested that smaller nanoparticles more readily penetrate the bacterial cell wall, disrupting essential cellular structures, functions, and inducing cell death.

The observed high susceptibility of *E. coli* in this study may also be explained by its thin peptidoglycan layer, a characteristic of Gram-negative bacteria, which allows easier access for MdSE-Ag/AgCl-NPs and makes them more vulnerable to internal structural damage.[66] In contrast, Gram-positive bacteria like *S. aureus* possess a thicker cell wall, which may provide added resistance to nanoparticle penetration and action.

Tolerance level (TL). The bactericidal or bacteriostatic nature of an antimicrobial agent can be evaluated by calculating its tolerance level, defined as the ratio of MBC to MIC. This value refers to the tolerance potential of an antimicrobial agent against selected pathogens. An inverse relationship is observed between the tolerance level and their pathogenicity. Following the standard classification, a TL value of ≤ 4 indicates a bactericidal effect, while a value ≥ 16 suggests a bacteriostatic response. The distinction lies in whether the agent actively kills the bacteria or merely inhibits their growth.

Table 4 Tolerance level (MBC/MIC) of selected bacterial strains treated with Medjool date seeds extract (MdSE), MdSE-Ag/AgCl-NPs, gentamicin, and $AgNO_3$

Treatments	Tolerance level[a]		
	E. coli (ATCC 25922)	*P. aeruginosa* (ATCC 27853)	*S. aureus* (ATCC 25923)
MdSE	2	4	8
MdSE-Ag/AgCl-NPs	2	2	2
Gentamicin	3.9	2	2
$AgNO_3$	1	2	2

[a] Tolerance values ≥ 16 indicate a bacteriostatic response, while values ≤ 4 reflect bactericidal activity.

Present study proves that the MdSE-Ag/AgCl-NPs exhibited TL values of 2 across all tested strains (*E. coli*, *P. aeruginosa*, and *S. aureus*), indicating strong bactericidal activity (Table 4). These findings support the assertion that phytofabricated silver nanoparticles using MdSE possess potent killing efficacy across both Gram-negative and Gram-positive bacteria. Numerous studies have similarly reported the bactericidal potential of seeds-derived biogenic AgNPs, with *Nigella sativa* and *Peganum harmala*-mediated AgNPs showing a TL values of $\sim$2 against *E. coli*, *S. aureus*, and *P. aeruginosa*.[73,74] This reinforces the relevance of MdSE-Ag/AgCl-NPs as promising bactericidal agents with broad-spectrum effectiveness.

The crude extract (MdSE) showed a broader tolerance range for *S. aureus*, with a TL of 8, followed by bactericidal TL values of 4 for *P. aeruginosa* and 2 for *E. coli*. While its effect remained bactericidal against *E. coli* and *P. aeruginosa*, the value of 8 for *S. aureus* suggests reduced killing efficiency, potentially indicating a shift toward a static effect in this strain. However, the tolerance ratios for all the 3 strains were achieved at substantially higher concentrations of the extract, unlike the MdSE-Ag/AgCl-NPs, which were effective at much lower concentrations. This highlights the enhanced potency gained through nanoparticle synthesis.

Silver nitrate ($AgNO_3$) recorded TL values of 1 for *E. coli* and 2 for both *P. aeruginosa* and *S. aureus*, indicating a consistent bactericidal profile. However, its known cytotoxic effects as discussed earlier may limit its practical applications despite its efficacy. Similarly, gentamicin, used as a positive standard control, also exhibited bactericidal activity, with TL values of 3.9 for *E. coli*, and 2 for *P. aeruginosa* and *S. aureus*, which validates the experiment.

***In vitro* biofilm inhibition assay.** Biofilms, which shield bacterial communities from external threats, are composed of a mixture of hydrophilic substances (proteins, nucleic acids,

and polysaccharides) and hydrophobic components (lipids and surfactants).[75,76] Among the materials under study, silver nanoparticles (AgNPs) have drawn significant interest for their ability to penetrate the protective matrix, disrupting biofilm integrity, and killing the bacterial cells. This action becomes possible, as it comes into close contact with the biofilms and are consistent with previous reports.[57,77] Guided by these findings, this study evaluated the antibiofilm potential of phytofabricated MdSE-Ag/AgCl nanoparticles in comparison with MdSE and positive standard control, gentamicin, as shown in Fig. 9.

To enable a fair and dose-dependent comparison, each treatment was tested at concentrations equivalent to 1/4, 1/2, 1, 2, and 4 times its respective MIC. For *E. coli*, MdSE-Ag/AgCl was evaluated at 0.010, 0.020, 0.039, 0.078, and 0.156 mg mL^{-1}, while for *P. aeruginosa* and *S. aureus*, it ranged from 0.020, 0.039, 0.078, 0.156, and 0.312 mg mL^{-1}. Gentamicin, used as a reference drug, was consistently tested across all strains at 0.0025, 0.005, 0.010, 0.020, and 0.039 mg mL^{-1}. The crude extract required much higher concentrations, ranging from 3.125, 6.25, 12.5, 25.0, and 50.0 mg mL^{-1} for *E. coli*, 1.563, 3.125, 6.25, 12.5, and 25.0 mg mL^{-1} for *P. aeruginosa*, and 0.781, 1.563, 3.125, 6.25, and 12.5 mg mL^{-1} for *S. aureus*, corresponding to 1/4, 1/2, 1, 2, and 4*MIC, respectively. This concentration-based approach allowed for detailed profiling of antibiofilm effects among treatments.

As depicted in Fig. 9, MdSE-Ag/AgCl-NPs demonstrated potent, concentration-dependent inhibition of biofilm formation across all tested strains. In *E. coli*, biofilm inhibition ranged from 15.38% at 1/4*MIC to 72.91% at 4*MIC. According to established criteria, where inhibition above 50% is regarded as good antibiofilm activity and values below 50% as poor activity,[78] the nanoparticles exhibited a good antibiofilm effect at concentrations of 1*MIC and above. Interestingly, at 2* and 4*MIC, no significant difference was observed between MdSE-Ag/AgCl-NPs and gentamicin at 1*MIC (70.72%) ($p > 0.05$), indicating a comparable antibiofilm effect between the biosynthesized nanoparticles and the conventional antibiotic at higher concentrations. In contrast, the crude MdSE extract only reached 45.93% inhibition at 4*MIC, falling into the poor activity range and showing significantly lower performance than the nanoparticle treatments ($p < 0.05$).

A similar trend was observed for *P. aeruginosa*, where MdSE-Ag/AgCl nanoparticles demonstrated even better biofilm eradication compared to their activity in *E. coli*. The nanoparticles achieved 73.57% inhibition at 1*MIC, surpassing the 50% threshold for good antibiofilm activity, and further increased to 90.77% inhibition at 2*MIC, which remained consistent through 4*MIC ($p > 0.05$). From 2* MIC onward, MdSE-Ag/AgCl nanoparticles exhibited biofilm inhibition levels exceeding 90%, and the differences compared to gentamicin were not statistically significant ($p > 0.05$). This suggests that the nanoparticles reached a near-complete biofilm disruption in *P. aeruginosa* as performed by gentamicin, without requiring further concentration increases. Meanwhile, the MdSE showed modest overall performance, with the extract exhibiting a delayed onset of efficacy, reaching the threshold for good antibiofilm activity only at 2*MIC (71.42%), and peaking at 82.13% inhibition at 4*MIC. However, despite this concentration-dependent improvement, inhibitory effect of MdSE remained significantly lower than that of the MdSE-Ag/AgCl-NPs across all tested concentrations ($p < 0.05$).

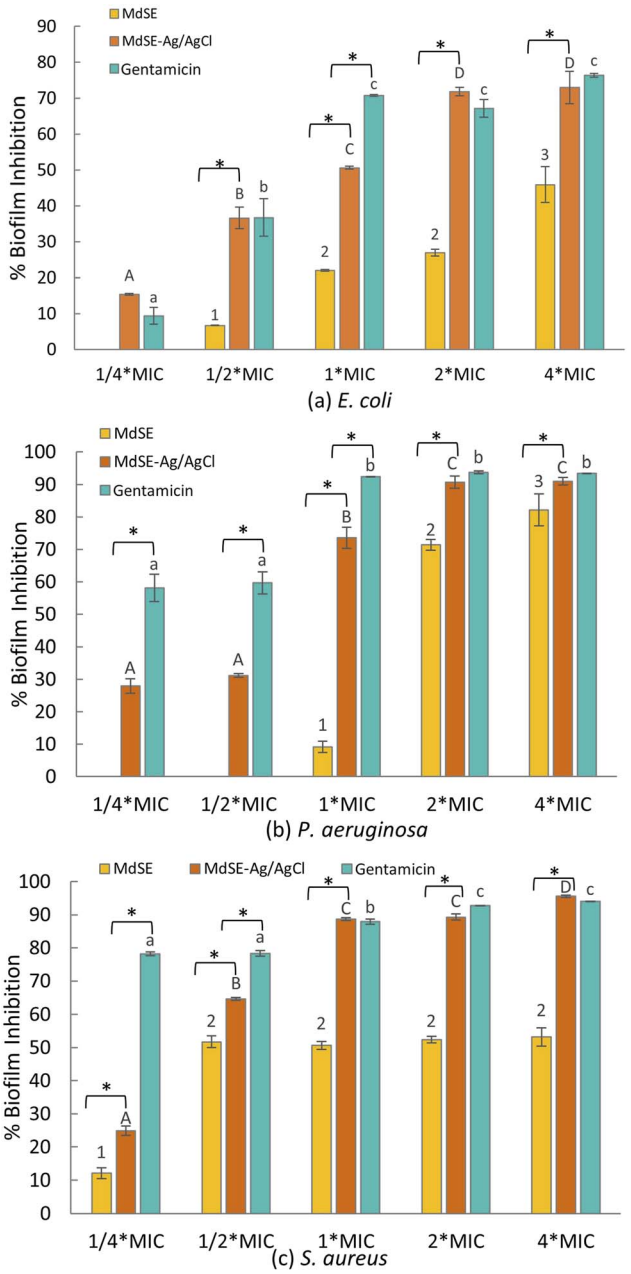

Fig. 9 Effect of Medjool date seeds extract (MdSE) (yellow bars), phytofabricated MdSE-Ag/AgCl-NPs (orange bars) and antibiotic gentamicin (positive standard control) (turquoise bars) on bacterial biofilm inhibition, evaluated on (a) *E. coli*, (b) *P. aeruginosa,* and (c) *S. aureus*. Results are expressed as mean ± standard deviation (SD). Statistical significance among treatments across various concentrations is indicated using uppercase letters, lowercase letters, and numerical values, respectively. The symbol (*) denotes significant differences ($p < 0.05$) observed when comparing each treatment with the MdSE-Ag/AgCl-NPs group. Tukey *post hoc* tests were used for multiple comparisons.

Among the three tested strains, *S. aureus* exhibited the most pronounced susceptibility to MdSE-Ag/AgCl-NPs. The nanoparticles achieved 64.54% inhibition even at 1/2*MIC, a level of antibiofilm activity not observed at sub-MIC concentrations in *E. coli* and *P. aeruginosa*, where inhibition remained below 50%. At 1*MIC, MdSE-Ag/AgCl-NPs reached 88.66% inhibition, maintaining this high level through 2*MIC ($p > 0.05$), and again demonstrating no statistically significant difference ($p > 0.05$) when compared to gentamicin at the same concentrations. This indicates that 1* or 2* MIC could serve as effective and preferable concentrations for practical application, offering substantial antibiofilm activity without the need to escalate dosing to 4*MIC. Concurrently, Mohanta *et al.* (2020)[79] reported a comparable inhibition level (~80%) using AgNPs synthesized from *Glochidion lanceolarium* at 80 μg mL^{-1}, closely aligning with the 88.66% inhibition achieved at 0.078 mg mL^{-1} (1*MIC) in the present study. In contrast to MdSE-Ag/AgCl-NPs, MdSE showed considerably lower antibiofilm performance against *S. aureus*. Its maximal inhibition of 53.18% at 4*MIC barely surpassed the threshold for good activity, and inhibition levels remained relatively unchanged with no significant difference between 1/2*MIC to higher doses. This plateau suggests that the extract alone lacked the concentration-responsive efficacy as demonstrated by the nanoparticle formulation, and significantly less functionable compared to MdSE-Ag/AgCl-NPs at all concentrations ($p < 0.05$) against *S. aureus*.

Comparatively, a study performed by Allemailem and his colleagues (2022)[23] reported the AgNPs synthesized using Ajwa variant date seeds extract to show <40% biofilm inhibition against *P. aeruginosa*, and ~70% for *S. aureus* and *E. coli* at 100 μg mL^{-1}. In contrast, MdSE-Ag/AgCl nanoparticles in this study achieved comparable or greater inhibition at just 78 μg mL^{-1}, indicating the enhanced antibiofilm potential with MdSE-based formulation. Biogenically synthesised Ag/AgCl-NPs from *O. ehrenbergii* (averagely 13.5 nm sized) showed nearly equivalent antibiofilm performance against *E. coli*, with ~54% inhibition at 31 μg mL^{-1}. This aligns closely with the 50.62% inhibition observed in our study at 39 μg mL^{-1} (1*MIC). Furthermore, the MdSE-based nanoparticles produced in this study presented enhanced biofilm inhibition compared to the discussed *O. ehrenbergii*-derived Ag/AgCl nanoparticles which recorded approximately 52% and 56% inhibition against *P. aeruginosa* and *S. aureus*, respectively, despite being tested at considerably higher concentrations of 250 μg mL^{-1} and 125 μg mL^{-1}.[10]

Overall, the findings from current experiment emphasizes MdSE-Ag/AgCl-NPs to possess potent antibiofilm performance even at lower concentrations, beginning at 1*MIC for Gram-negative bacteria (*E. coli* and *P. aeruginosa*) and 1/2*MIC for *S. aureus*. This, in many instances matched the efficacy of gentamicin (especially at 2*MIC and 4*MIC), while consistently outperforming the crude extract. The incorporation of bioactive components from Medjool seeds extract during the synthesis may have improved nanoparticle stability and silver ion release which may have interfered with the gene expression in charge of biofilm formation,[80] without compromising biocompatibility. Hence, this study suggests MdSE-Ag/AgCl-NPs as a promising natural alternative for the management of biofilm-associated infections.

Conclusion

Current study demonstrates the potential of Medjool date seeds extract as an effective natural precursor for the green synthesis of Ag/AgCl nanoparticles. The biosynthesized nanoparticles exhibited antibacterial activity against both Gram-negative and Gram-positive pathogens, as confirmed through MIC, MBC, and TL evaluations. Additionally, the MdSE-Ag/AgCl-NPs showed promising antibiofilm effects, suggesting their potential in disrupting biofilm-associated infections. These results support the use of Medjool seeds extract in developing eco-friendly nanomaterials with enhanced antimicrobial performance.

Data availability

The data analysed for selected area electron diffraction (SAED) using ImageJ software and results obtained for antibiofilm activity were provided in this document as part of the ESI.† All other data generated or analyzed during this study are included in the article.

Author contributions

Pushpa Thirubuvanesvari-Duraivelu: Research design, methodology development, data curation, formal analysis, investigation, original draft preparation, manuscript review, and editing. Siti Salwa Abd Gani: Supervision, project administration, validation, and critical review. Masriana Hassan: Supervision and contribution to methodological design. Mohd Izuan Effendi Halmi: Statistical analysis and data interpretation. Reem Fawaz Abutayeh, Mohammad A. A. Al-Najjar, and Ala' Abu-Odeh: Project and funding administration, as well as manuscript review. All authors have read and approved the final version of the manuscript for publication.

Conflicts of interest

The authors declare that there is no conflict of interest.

Acknowledgements

This study was supported with the funding from MyBrainSc provided by the Malaysian Ministry of Higher Education and the Universiti Putra Malaysia (UPM) – Applied Science Private University (ASU), Jordan Matching Grant (Project Code: UPM-JORDAN/2022/9300491).

References

1 J. Mussin, V. Robles-Botero, R. Casañas-Pimentel, F. Rojas, L. Angiolella, E. S. Martin-Martinez and G. Giusiano, *Sci. Rep.*, 2021, **11**, 14566.
2 H. B. H. Rahuman, R. Dhandapani, S. Narayanan, V. Palanivel, R. Paramasivam, R. Subbarayalu,

S. Thangavelu and S. Muthupandian, *IET Nanobiotechnol.*, 2022, **16**, 115–144.
3 K. N. Agey, P. P. Mahabdi and D. Prajapati, *J. Ayurveda Integr. Med. Sci.*, 2024, **9**, 98–103.
4 M. K. Rai, S. D. Deshmukh, A. P. Ingle and A. K. Gade, *J. Appl. Microbiol.*, 2012, **112**, 841–852.
5 P. Bhuyar, M. H. A. Rahim, S. Sundararaju, R. Ramaraj, G. P. Maniam and N. Govindan, Beni-Suef Univ. J, . *Basic Appl. Sci.*, 2020, **9**, 1–15.
6 A. E. Adebayo, A. M. Oke, A. Lateef, A. A. Oyatokun, O. D. Abisoye, I. P. Adiji, D. O. Fagbenro, T. V. Amusan, J. A. Badmus, T. B. Asafa, L. S. Beukes, E. B. Gueguim-Kana and S. H. Abbas, *Nanotechnol. Environ. Eng.*, 2019, **4**, 1–15.
7 F. Lu, Y. Liu, Y. Dai, G. Zhang and Y. Tong, *RSC Adv.*, 2025, **15**, 6357–6369.
8 A. Naganthran, G. Verasoundarapandian, F. E. Khalid, M. J. Masarudin, A. Zulkharnain, N. M. Nawawi, M. Karim, C. A. C. Abdullah and S. A. Ahmad, *Materials*, 2022, **15**, 427.
9 S. Ahmadi, M. Fazilati, S. M. Mousavi and H. Nazem, *J. Exp. Nanosci.*, 2020, **15**, 363–380.
10 Z. Hachem, R. Kashmar, A. M. Abdallah, R. Awad and M. I. Khalil, *Results Mater*, 2024, **21**, 100550.
11 N. Sultana, M. Ruhul-Amin, I. Hasan, S. R. Kabir and A. K. M. Asaduzzaman, *Food Chem. Adv.*, 2024, **4**, 100709.
12 S. R. Kabir, A. K. M. Asaduzzaman, R. Amin, A. T. Haque, R. Ghose, M. M. Rahman, J. Islam, M. B. Amin, I. Hasan, T. Debnath, B. Chun, X. Zhao, M. Khalilur Rahman Khan and M. T. Alam, *ACS Omega*, 2020, **5**, 20599–20608.
13 Y. Zhou, R. Chen, T. He, K. Xu, D. Du, N. Zhao, X. Cheng, J. Yang, H. Shi and Y. Lin, *ACS Appl. Mater. Interfaces*, 2016, **8**, 15067–15075.
14 Y. Zhu, H. Liu, L. Yang and J. Liu, *Mater. Res. Bull.*, 2012, **47**, 3452–3458.
15 S. Kota, P. Dumpala, R. K. Anantha, M. K. Verma and S. Kandepu, *Sci. Rep.*, 2017, **7**, 11566.
16 K. Okaiyeto, M. O. Ojemaye, H. Hoppe, L. V. Mabinya and A. I. Okoh, *Molecules*, 2019, **24**, 4382.
17 Y. Gorshkova, M. E. Barbinta-Patrascu, G. Bokuchava, N. Badea, C. Ungureanu, A. Lazea-Stoyanova, M. Răileanu, M. Bacalum, V. Turchenko, A. Zhigunov and E. Juszyńska-Gałązka, *Nanomaterials*, 2021, **11**, 1811.
18 Statista, **https://www.statista.com/statistics/960247/dates-production-worldwide/**, accessed April 2025.
19 L. Borsacchi, C. Vita and P. Pinelli, *Preprints*, 2025, DOI: **10.20944/preprints202501.0797.v1**.
20 M. Ranasinghe, I. Manikas, S. Maqsood and C. Stathopoulos, *Sustainability*, 2022, **14**, 605.
21 S. Maqsood, O. Adiamo, M. Ahmad and P. Mudgil, *Food Chem.*, 2020, **308**, 125522.
22 E. D. T. Bouhlali, A. Hmidani, B. Bourkhis, T. Khouya, M. Ramchound, Y. Filali-Zegzoutib and C. Alem, *Heliyon*, 2020, **6**, e03436.
23 K. S. Allemailem, H. Khadri, M. Azam, M. A. Khan, A. H. Rahmani, F. Alrumaihi, R. Khateef, M. Azam Ansari, E. A. Alatawi, M. H. Alsugoor, N. M. Almansour, B. Y. Alhatlani and A. Almatroudi, *Appl. Sci.*, 2022, **12**, 4537.
24 S. Z. A. Khader, S. S. Z. Ahmed, M. R. Mahboob, S. B. Prabaharan, S. O. Lakshmanan, K. R. Kumar and D. David, *Braz. J. Pharm. Sci.*, 2022, **58**, e18594.
25 M. Khatami and S. Pourseyedi, *IET Nanobiotechnol.*, 2015, **9**, 184–190.
26 P. Thirubuvanesvari-Duraivelu, S. S. A. Gani, M. Hassan, M. I. E. Halmi, R. F. Abutayeh and M. A. Al-Najjar, *Bull. Chem. Soc. Ethiop.*, 2024, **38**, 547–562.
27 Clinical and Laboratory Standards Institute (CLSI), *Methods for Dilution Antimicrobial Susceptibility Tests for Bacteria that Grow Aerobically*, Clinical and Laboratory Standards Institute, Wayne, PA, 2018, 10th edn M07-A11.
28 M. R. Trisha, V. D. Gunawan, J. X. Wong, M. S. P. Dek and Y. Rukayadi, *Heliyon*, 2024, **10**, e35691.
29 H. Barabadi, O. Hosseini, K. Jounaki, S. Sadeghian-Abadi, F. Ashouri, A. M. A. Alrikabi, H. Vahidi, S. Amidi, F. Mojab, N. Mohammadi and E. Mostafavi, *Mater. Adv.*, 2023, **4**, 3037–3054.
30 S. S. Dash, S. Samanta, S. Dey, B. Giri and S. K. Dash, *Biol. Trace Elem. Res.*, 2020, **198**, 681–696.
31 N. Talank, H. Morad, H. Barabadi, F. Mojab, S. Amidi, F. Kobarfard, M. A. Mahjoub, K. Jounaki, N. Mohammadi, G. Salehi, M. Ashrafizadeh and E. Mostafavi, *Talanta*, 2022, **243**, 123374.
32 H. Barabadi, F. Mojab, H. Vahidi, B. Marashi, N. Talank, O. Hosseini and M. Saravanan, *Inorg. Chem. Commun.*, 2021, **129**, 108647.
33 K. A. A. A. Rahim and A. M. A. Mohamed, *Jundishapur J. Microbiol.*, 2015, **8**, e25867.
34 X. F. Zhang, Z. G. Liu, W. Shen and S. Gurunathan, *Int. J. Mol. Sci.*, 2016, **17**, 1534.
35 M. M. Alanazi, *J. King Saud Univ. Sci.*, 2024, **36**, 103312.
36 M. Adnan, A. J. Siddiqui, S. A. Ashraf, M. S. Ashraf, S. O. Alomrani, M. Alreshidi, B. Tepe, M. Sachidanandan, C. Danciu and M. Patel, *Antibiotics*, 2023, **12**, 1415.
37 Z. Zaheer, *J. Photochem. Photobiol. B.*, 2018, **178**, 584–592.
38 D. Bamal, A. Singh, G. Chaudhary, M. Kumar, M. Singh, N. Rani, P. Mundlia and A. R. Sehrawat, *Nanomaterials*, 2021, **11**, 2086.
39 B. Rao and R. C. Tang, *Adv. Nat. Sci.: Nanosci. Nanotechnol.*, 2017, **8**, 015014.
40 Hemlata, P. R. Meena, A. P. Singh and K. K. Tejavath, *ACS Omega*, 2020, **5**, 5520–5528.
41 Y. K. Mohanta, S. K. Panda, A. K. Bastia and T. K. Mohanta, *Front. Microbiol.*, 2017, **8**, 626.
42 A. Qidwai, R. Kumar and A. Dikshit, *Green Chem. Lett. Rev.*, 2018, **11**, 176–188.
43 F. M. Aldayel, M. S. Alsobeg and A. Khalifa, *Braz. J. Biol.*, 2021, **82**, e242301.
44 R. Singh, R. Singh, P. Parihar and J. V. Mani, *Process Biochem.*, 2024, **143**, 337–352.
45 K. D. Mekonnen, *Heliyon*, 2023, **9**, e14699.
46 S. Zafar and A. Zafar, *Open Biotechnol. J.*, 2019, **13**, 37–46.
47 N. Kumar, I. Khangwal and A. Upadhyay, *Discov. Food*, 2024, **4**, 1–12.
48 M. E. Abdel-Alim, K. Samaan, D. Guillaume and H. Amla, *Bioactivities*, 2023, **1**, 1–8.

49 H. Arshad, M. A. Sami, S. Sadaf and U. Hassan, *Sci. Rep.*, 2021, **11**, 5996.
50 D. Acharya, K. M. Singha, P. Pandey, B. Mohanta, J. Rajkumari and L. P. Singha, *Sci. Rep.*, 2018, **8**, 201.
51 S. Farhadi, B. Ajerloo and A. Mohammadi, *Acta Chim. Slov.*, 2017, **64**, 129–143.
52 A. Arya, P. K. Tyagi, S. Bhatnagar, R. K. Bachheti, A. Bachheti and M. Ghorbanpour, *Sci. Rep.*, 2024, **14**, 7243.
53 R. Soundharajan and H. Srinivasan, *Aquac. Int.*, 2025, **33**, 1–19.
54 T. B. Devi, M. Ahmaruzzaman and S. Begum, *New J. Chem.*, 2016, **40**, 1497–1506.
55 N. Stozhko, A. Tarasov, V. Tamoshenko, M. Bukharinova, E. Khamzina and V. Kolotygina, *Physchem*, 2024, **4**, 402–419.
56 M. T. Yassin, A. A. F. Mostafa, A. A. Al-Askar and F. O. Al-Otibi, *Crystals*, 2022, **12**, 603.
57 F. Maryani and A. W. Septama, *Mater. Adv.*, 2022, **3**, 8267–8275.
58 A. Sidorowicz, T. Szymański and J. D. Rybka, *Biology*, 2021, **10**, 784.
59 E. Ismail, A. Diallo, M. Khenfouch, S. M. Dhlamini and M. Maaza, *J. Alloys Compd.*, 2016, **662**, 283–289.
60 R. Varghese, M. A. Almalki, S. Ilavenil, J. Rebecca and K. C. Choi, *Saudi J. Biol. Sci.*, 2019, **26**, 148–154.
61 A. Abizi-Moqadam, S. Mortazavi-Derazkola, M. Zare-Bidaki, F. Osmani and L. Alizadeh, *Curr. Pharm. Biotechnol.*, 2025, **26**, e13892010349133.
62 E. Parthiban, N. Manivannan, R. Ramanibai and N. Mathivanan, *Biotechnol. Rep.*, 2019, **21**, e00297.
63 A. K. Jha, S. Zamani and A. Kumar, *Biotechnol. Appl. Biochem.*, 2022, **69**, 1653–1662.
64 M. Younas, M. H. Rasool, M. Khurshid, A. Khan, M. Z. Nawaz, I. Ahmad and M. N. Lakhan, *Biochem. Syst. Ecol.*, 2023, **107**, 104605.
65 A. P. Ananda, H. M. Manukumar, N. B. Krishnamurthy, B. S. Nagendra and K. R. Savitha, *Microb. Pathog.*, 2019, **126**, 27–39.
66 C. Vanlalveni, K. Rajkumari, J. Das, S. Tuteja and V. D. Veeranki, *Environ. Chem. Lett.*, 2021, **19**, 1291–1310.
67 J. Mussin, V. Robles-Botero, R. Casañas-Pimentel, F. Rojas, L. Angiolella, E. San Martin-Martinez and G. Giusiano, *Sci. Rep.*, 2021, **11**, 14566.
68 Y. G. Yuan, Q. L. Peng and S. Gurunathan, *Int. J. Mol. Sci.*, 2017, **18**, 569.
69 Y. Wu, Y. Yang, Z. Zhang, Z. Wang, Y. Zhao and L. Sun, *Adv. Powder Technol.*, 2018, **29**, 407.
70 S. Shaikh, N. Nazam, S. M. D. Rizvi, K. Ahmad, M. H. Baig, E. J. Lee and I. Choi, *Int. J. Mol. Sci.*, 2019, **20**, 2468.
71 J. Y. Cheon, S. J. Kim, Y. H. Rhee, O. H. Kwon and W. H. Park, *Int. J. Nanomedicine*, 2019, **14**, 2773–2780.
72 Y. Y. Loo, Y. Rukayadi, M. A. R. Nor-Khaizura, C. H. Kuan, B. W. Chieng, M. Nishibuchi and S. Radu, *Front. Microbiol.*, 2018, **9**, 1555.
73 H. Al-Momani, M. Almasri, D. A. Al Balawi, S. Hamed, B. A. Albiss, N. Aldabaibeh, L. Ibrahim, H. Albalawi, S. A. H. Mahmoud, A. I. Khasawneh, M. Kilani, M. Aldhafeeri, M. Bani-Hani, M. Wilcox, J. Pearson and C. Ward, *Sci. Rep.*, 2023, **13**, 8876.
74 A. Almatroudi, H. Khadri, M. Azam, A. H. Rahmani, F. K. A. Khaleefah, R. Khateef, M. A. Ansari and K. S. Allemailem, *Processes*, 2020, **8**, 388.
75 L. Karygianni, Z. Ren, H. Koo and T. Thurnheer, *Trends Microbiol.*, 2020, **28**, 668–681.
76 S. J. Kassinger and M. L. V. Hoek, *Synth. Syst. Biotechnol.*, 2020, **5**, 1–10.
77 A. S. Joshi., P. Singh and I. Mijakovic, *Int. J. Mol. Sci.*, 2020, **21**, 7658.
78 R. O. Adeyemo, I. M. Famuyide, J. P. Dzoyem and M. L. Joy, *Evid. Based. Complement. Alternat. Med.*, 2022, **2022**, 1307801.
79 Y. K. Mohanta, K. Biswas, S. K. Jena, A. Hashem, E. F. A. Allah and T. K. Mohanta, *Front. Microbiol.*, 2020, **11**, 1143.
80 P. Singh, S. Pandit, M. Beshay, V. R. S. S. Mokkapati, J. Garnaes, M. E. Olsson, A. Sultan, A. Mackevica, R. V. Mateiu, H. Lütken, A. E. Daugaard, A. Baun and I. Mijakovic, *Artif. Cells Nanomed. Biotechnol.*, 2018, **46**, 886–899.